MJFAS
Malaysian Journal of Fundamental and Applied Sciences

Kadhim *et al.* | Malaysian Journal of Fundamental and Applied Sciences, Vol. 22 (2026) 917–927

RESEARCH ARTICLE

Computational Evaluation of Gamma-Ray, Electron, and Fast-Neutron Shielding Properties of PMMA/Bi_2O_3/ZnO Nanocomposites

Oday J. K. Kadhim[a], Najlaa Jerjack Abdullah[a], N Nadia[a], Mohammed J. R. Aldhuhaibat[a], and A.A. Salim[b,c*]

[a]Department of Physics, College of Science, Wasit University, Wasit, Iraq; [b]Laser Center & Physics Department, Faculty of Science, Universiti Teknologi Malaysia, 81310 UTM Johor Bahru, Johor, Malaysia; [c]Department of Laser and Optoelectronics Engineering, College of Engineering, University of Kut, Wasit, 52001, Iraq

Abstract This computational study determined the radiation-shielding properties of five theoretically formulated polymethyl methacrylate (PMMA)-based nanocomposites, denoted as P1 to P5 reinforced with varying concentrations of bismuth oxide (Bi_2O_3) and zinc oxide (ZnO) nanopowders. The proposed nanocomposites followed the formula as 80PMMA-(20-x)Bi_2O_3-xZnO, with x = 2, 6, 10, 14, and 18 wt.%. The attenuation properties of these materials were theoretically evaluated against diverse ionizing radiations, including gamma rays, beta particles, and fast neutrons across a broad energy spectrum. The mass attenuation and mass energy absorption coefficients of the nanocomposites were determined within the gamma-ray energy range of 1 keV to 20 MeV. The radiation shielding efficiency, specific gamma-ray constant, and irradiation dose rate were obtained through the NIST Standard Reference Database 126. The electron stopping power of the nanocomposites was computed by the ESTRA code for electron energies between 0.1 and 100 MeV, while the neutron shielding potential was evaluated via the fast neutron removal cross-section. Comparative analysis was conducted with conventional shielding materials such as boron carbide, graphite, and polyethylene using the Phy-X/PSD online program. The calculations demonstrated that the nanocomposite with the highest Bi_2O_3 content exhibited superior shielding efficiency against gamma rays, particularly in low and medium energy ranges. Furthermore, all nanocomposites showed effective attenuation of high-energy electrons, while the highest ZnO content revealed the highest shielding effectiveness against fast neutrons. These findings indicate that the significant potential of PMMA-based Bi_2O_3/ZnO nanocomposites as advanced materials has considerable value for the development of high-performance radiation shielding in a variety of applications involving ionizing radiation.

Keywords: Gamma ray, nanocomposite, electrons, fast neutron, shielding, electron stopping power.

***For correspondence:**
asali@utm.my

Received: 15 May 2026
Accepted: 05 August 2026

© Copyright Kadhim. This article is distributed under the terms of the Creative Commons Attribution License, which permits unrestricted use and redistribution provided that the original author and source are credited.

Introduction

The increasing utilization of ionizing radiation across diverse industrial, agricultural, and medical sectors has posed significant concerns due to its potential impact on the environment and living organisms [1-3]. The harmful effects of ionizing radiation, particularly in high-exposure settings, have demanded the implementation of stringent protective measures to mitigate risks for personnel working with radiological technologies. To minimize radiation exposure, it is critical to reduce both the exposure duration and the

proximity of workers to radiation sources [4]. This can be effectively achieved through the strategic deployment of radiation shielding materials, which act as barriers to limit the transmission of harmful radiation and ensure the safety of workers and the surrounding environment [5]. Due to its high density and atomic number, lead has been the preferred material for radiation shielding, which provides effective attenuation of ionizing radiation. It is a heavy and toxic material that can severely be affected by the mechanical and environmental features [1]. Despite its efficacy, lead presents significant drawbacks, including its toxicity, weight, and vulnerability to degradation under mechanical and environmental stressors. Consequently, there has been a concerted effort to explore alternative shielding materials that provide comparable or greater protective performance without the environmental and health hazards associated with lead.

Numerous studies have focused on the development of novel shielding materials, particularly composite materials, which combine polymers with various oxide powders to enhance radiation attenuation properties [6]. These composites are engineered to provide high shielding efficiency while maintaining mechanical stability and environmental durability. The suitability of these new materials changes depending on the specific type and energy and operational conditions of the radiation in which the shielding is used. Researchers have made significant strides in examining the effect of multiple reinforcement materials on the physical and radiological properties of various polymer matrices, including epoxy composites, polyethylene, and polymeric nanocomposites [7-9]. For example, the incorporation of nanoparticles (NPs) or metal oxide fillers into polymeric matrices has been shown to improve the radiation shielding properties, offering a lightweight, effective alternative to lead-based shields. In addition, the adaptability of these composites to different radiation types such as gamma rays, X-rays, and neutrons has been rigorously investigated to optimize their performance in specific industrial and medical applications [10]. Li et al. fabricated PMMA/MWCNT nanocomposites and determined their ionizing radiation shielding properties. The results demonstrated that the addition of MWCNTs to the PMMA matrix can further lower the secondary neutron generation of the pure polymer, but no obvious change was seen in the proton transmission property [11]. Bel et al. used PMMA/CMT composites as a shield against γ-rays and neutrons wherein the values of the attenuation coefficient, half-value layer, and neutron transmission were evaluated. It was shown that the enhancement of colemanite $Ca_2B_6O_{11}5H_2O$ (CMT) for PMMA can improve the radiation protection capacity of the Cs-137 gamma source and neutrons emitted from the Pu-Be neutron source [12]. Cao et al. studied the gamma-ray shielding ability, as well as the physical and mechanical properties of PMMA/Bi_2O_3 composites containing 0-44.0 wt% bismuth trioxide. The findings revealed that the high loading of Bi_2O_3 in the composites can greatly improve their micro-hardness.

It has been reported that these composites are potential materials for radiation shielding [13]. Various studies were conducted to calculate the stopping power of electrons and alpha particles in different materials to determine their radiation shielding potential [14-19]. Considering the significance of strong shielding materials development against diverse ionizing radiations, a theoretical study was conducted to propose some new nanocomposite formulations made from polymethyl methacrylate polymer (PMMA) reinforced with zinc oxide (ZnO) and bismuth oxide (Bi_2O_3) nanopowders at different concentrations. The radiation shielding capacities of these nanocomposites against gamma rays, beta particles (electrons), and fast neutrons were evaluated. The nuclear radiation attenuation properties of the proposed PMMA-based nanocomposites were meticulously evaluated and subsequently compared to the performance of existing state-of-the-art shielding materials. This comparison provides valuable insight into the potential advantages of these new nanocomposites for radiation protection applications.

Previous studies have demonstrated the potential of Bi_2O_3- and ZnO-containing composites as effective radiation shielding materials due to the high atomic number of bismuth and the favorable structural properties of ZnO. Bi_2O_3 was chosen as the principal high-Z filler due to the high atomic number of bismuth (Z=83), which enhances photon attenuation, particularly at low photon energies where photoelectric absorption is dominant. ZnO was incorporated as a lower-Z oxide filler to tune the Bi_2O_3/ZnO ratio and tune the density and elemental composition of the PMMA-based nanocomposites. Partial substitution of Bi_2O_3 with ZnO is expected to reduce the contribution of high-Z bismuth to radiative electron energy loss, including bremsstrahlung production, while allowing the shielding response to be evaluated over different radiation types [5]. Yasser et al. [20] investigated PMMA/ZnO/Bi_2O_3 hybrid nanocomposites; their work mainly addressed the mechanical characteristics and general radiation attenuation behavior of the prepared composites. In contrast, the present study provides a more detailed theoretical assessment of the shielding parameters, including MAC, LAC, HVL, MFP, Zeff, and Neff, with emphasis on the influence of nanoparticle composition on photon interaction mechanisms. The combination of PMMA, Bi_2O_3, and ZnO provides a compositional approach for examining the balance between photon attenuation, electron stopping behavior, and fast-neutron removal. In the present computation, Bi_2O_3 is regarded as the primary component responsible for enhanced gamma-ray

attenuation. ZnO is employed to provide compositional tunability and to investigate the trade-off between photon/electron attenuation and fast-neutron removal, rather than as a direct substitute expected to improve all shielding parameters simultaneously.

The primary motivation of this study is the development of lightweight, non-toxic, and multifunctional radiation shielding materials based on PMMA-Bi_2O_3-ZnO nanocomposites for mixed radiation environments such as high-energy radiotherapy facilities and nuclear-related applications. The research addressed the challenge of developing shielding materials capable of simultaneously attenuating different types of ionizing radiation, including gamma rays, secondary fast neutrons, and electrons (beta particles), which may be generated in modern clinical particle accelerator systems. By combining the high atomic number properties of bismuth for enhanced photon attenuation, the compositional advantages of zinc oxide for tuning radiation interaction behavior, and the hydrogen-rich PMMA matrix for neutron moderation, the proposed nanocomposite system provides a potential alternative to conventional lead-based shielding materials. This approach aimed to achieve effective radiation protection while reducing concerns associated with the toxicity, weight, and environmental impact of lead-based shields in medical radiation protection and precision nuclear engineering applications.

Computational Methodology

To access the ionizing radiation shielding power of a material, the transmission of gamma rays through it was analysed. The linear attenuation coefficient (μ) in units of cm^{-1} was acquired using the Lambert-Beer law given by [21]:

$$I = I_o\, e^{-\mu x} \tag{1}$$

where x is the thickness of the material, and I and I_o are the corresponding initial and transmitted photon intensities. The mass attenuation coefficient (μ/ρ) of the material in units of cm^2/g was acquired by dividing its linear attenuation coefficient by the density:

$$I = I_o\, e^{-(\mu/\rho)\rho x} \tag{2}$$

The value of μ/ρ for any chemical substance or mixture of elements can be obtained using [22]:

$$\mu/\rho = \sum_i w_i\, (\mu/\rho)_i \tag{3}$$

where w_i and $(\mu/\rho)_i$ are the fraction weight and mass attenuation coefficient of the i^{th} element. If one uses the radiation dose rate (D) instead of the radiation intensity (I) in equation (1), the linear and mass attenuation coefficient in equations (1), (2), and (3) can be replaced by the linear (μ_{en}) and mass (μ_{en}/ρ) energy absorption coefficients, respectively [23, 24].

The true density is referred to the ratio of the mass of a substance to its true volume without pores or voids. The theoretical density of a compound or mixture (ρ_c) can be obtained via [25,26]:

$$\boldsymbol{\rho_c = 1/\sum_i w_i/\rho_i} \tag{4}$$

where ρ_i and w_i represent the theoretical density and the weight fraction of the i^{th} element of the compound, respectively. The molar volume (VM) of any compound can be obtained from the total molecular weight (MT) via [27,28]:

$$V_M = M_T/\rho \tag{5}$$

The radiation protection efficiency (RPE) for any radiative shield is evaluated by [29]:

$$RPE = (1 - e^{-\mu x}) \times 100\% \tag{6}$$

The specific γ-ray constant (Γ) can be obtained from the photons exposure rate of energy Eγ emitted from a radioactive source with activity 1Ci placed 1 m away from the target material using [30]:

$$\Gamma = 657.68 \times E_\gamma \frac{\mu_{en}}{\rho}\ \left(\frac{R.m^2}{Ci.hr}\right) \tag{7}$$

The irradiation dose (D) can be computed using [29]:

$$D = \frac{\Gamma A t}{r^2} \quad (8)$$

where A is the activity of radioactive source, t is the total time of exposure, and r refer to the distance of the radioactive source.

It is established that the energy loss and stopping power of charged particles in various materials like air, tissues, and polymers play a significant role for different applications in the fields of particle physics, nuclear physics, radiation doses and damage, radiotherapy, and radiochemistry [31-33]. The stopping power of a shield can be expressed as the average energy loss over unit path length, which depends on the nature of the target material and projectile's velocity as well as charge [34, 35].

The Bethe relativistic quantum mechanical equation for heavy charged particles can well describe their mass stopping power in a uniform medium [35]:

$$\frac{-dE}{\rho dx} = \frac{4\pi k_0^2 e^4 z^2 Z N_A}{mc^2 \beta^2 A}\left[\ln\left(\frac{2mc^2\beta^2}{I(1-\beta^2)}\right) - \beta^2\right] \quad (9)$$

where k_0, Z, z, A, β, ρ, and I are the Boltzman constant, atomic number of the absorber, atomic number of the incoming charged particle, atomic mass, relative velocity (v/c) of the particle, absorber density, and absorber mean ionization potential, respectively.

When heavily charged particles traverse through matter, they lose energy mainly via the process of ionization and excitation of atoms in the medium [36, 37]. The kinetic energy of the traversing charged particles reduces either via elastic collisions with electrons (collision loss) or inelastic collisions with bremsstrahlung photons (radiative loss). Therefore, the total mass stopping power for the electron interactions can be written in two parts:

$$\frac{-dE}{\rho dx} = \left(\frac{-dE}{\rho dx}\right)_{col} + \left(\frac{-dE}{\rho dx}\right)_{rad} \quad (10)$$

where the first and second terms are the corresponding collision and radiative mass stopping power. They can be calculated using the kinetic energy of a particle (T) by:

$$\left(\frac{-dE}{\rho dx}\right)_{col} = \left(\frac{4\pi k_0^2 e^4 Z N_A}{mc^2\beta^2 A}\right)\left[\frac{T(T+mc^2)\beta^2}{2I^2mc^2} + (1-\beta^2) - \left(2\sqrt{1-\beta^2} - 1 + \beta^2\right)\ln 2 - \frac{1}{2}\left(1-\sqrt{1-\beta^2}\right)^2\right] \quad (11)$$

$$\left(\frac{-dE}{\rho dx}\right)_{rad} = \left[\frac{k_0^2 e^4 Z^2 N_A (T+mc^2)}{137 m^2 c^4 A}\right]\left[4\ln\frac{2(T+mc^2)}{mc^2} - \frac{4}{3}\right] \quad (12)$$

The total neutron removal cross-section (∑R) is a measure of the interaction probabilities of neutrons in the limit homogeneous material. The value of ∑R for every constituent element in the proposed nanocomposites was calculated via [37-39]:

$$\sum R = \sum_i w_i (\sum R/\rho)_i \quad (13)$$

where wi the fractional density and ΣR/ρ is the mass removal cross-section of i^{th} element [40]. In the present work, Phy-X/PDS program was used to obtain the effective removal cross-sections for the elements, compounds, and mixtures [41].

Results and Discussions

Figure 1 shows the variation of density and molar volume as a function of ZnO concentration" would be more appropriate. The density and molar volume of the composites were decreased from 1.146469 to 1.129502 g/cm³ and 144.4378 to 92.12991 cm³/mol when the ZnO concentration changed from 2 to 18 wt%, respectively. The obtained decrease in the density can mainly be due to the substitution of higher molecular weight Bi_2O_3 contents (465.957 g/mol) by the lower molecular weight ZnO (81.379 g/mol). Accordingly, the total molecular weight of the samples was lowered from 165.5934 to 104.061 g/mol. Table 1 shows the compositions, codes, and physical properties of the proposed nanocomposites.

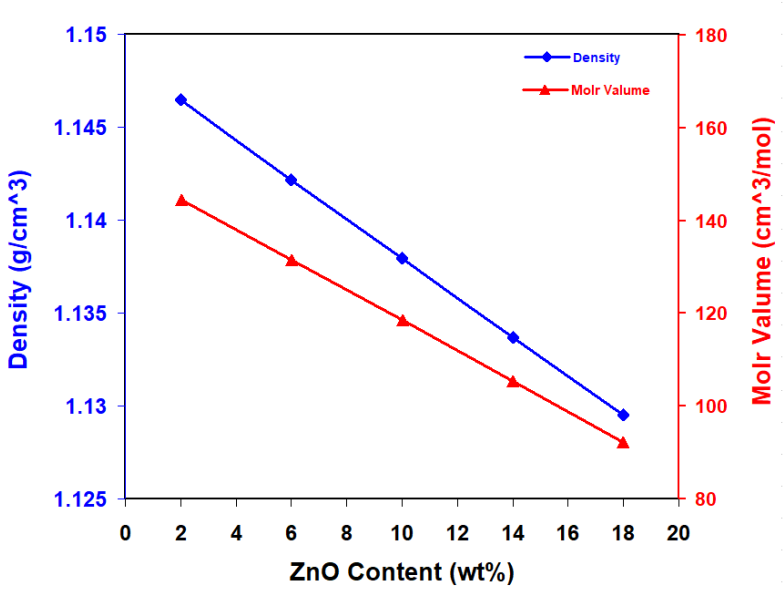


Figure 1. ZnO concentration-dependent variation in the densities and molar volumes of the studied nanocomposites.

Table 1. Values of wt% and mol% content, ρ, M_T, V_M and codes of the nanocomposites.

Sample codes	Components						ρ (g/cm^3)	M_T (g/mol)	V_M (cm^3/mol)
	PMMA		ZnO		Bi_2O_3				
	wt%	mol%	wt%	mol%	wt%	mol%			
P1	80	92.66976	2	2.850188	18	4.480047	1.146469	165.5934	144.4378
P2	80	88.50574	6	8.166353	14	3.327909	1.14218	150.2103	131.512
P3	80	84.69983	10	13.02531	10	2.274859	1.137922	134.8272	118.4854
P4	80	81.20775	14	17.48361	6	1.308642	1.133697	119.4441	105.358
P5	80	77.99222	18	21.58884	2	0.418941	1.129502	104.061	92.12991

Mass attenuation coefficient and radiation protection efficiency

Figure 2 illustrates the γ-ray energy-dependent mass attenuation coefficients (μ/ρ) of the nanocomposites. The values of μ/ρ and μ_{en}/ρ of the PMMA polymer and the O, Zn, Bi compounds were obtained from the NIST Standard Reference Database 126 [42]. These data were then utilized to obtain the mass attenuation and mass energy absorption coefficients of the nanocomposites by equation (3). These values were decreased noticeably with the increase in the γ-ray energies. The coefficient was very large for the nanocomposite P1 at all energies. The variation of the mass attenuation coefficient (μ/ρ) with photon energy can be explained based on the fundamental photon interaction mechanisms occurring within the nanocomposite system. At low photon energies, particularly below several hundred keV, photoelectric absorption represents the dominant interaction process. Since the probability of photoelectric absorption strongly increases with atomic number, the higher Bi_2O_3-containing nanocomposites exhibit greater attenuation capability due to the high atomic number of bismuth (Z = 83), which contributes to increasing the effective atomic number (Zeff) of the composite system. This effect is particularly evident in the low-energy region, where the difference between the investigated compositions becomes more pronounced. As the photon energy increases into the intermediate-energy region (0.1–5 MeV), Compton scattering becomes the dominant photon interaction mechanism. Unlike the photoelectric effect, Compton scattering depends mainly on the electron density of the material rather than strongly on atomic number; therefore, the differences in μ/ρ among the nanocomposite formulations become less significant in this region. At higher photon energies above the pair-production threshold (1.022 MeV), pair production gradually contributes to photon attenuation. Although the overall attenuation coefficient decreases with increasing photon energy, the composites containing higher Bi_2O_3 concentration maintain relatively higher attenuation values due to the enhanced contribution of high-Z

bismuth to photon interactions. These results demonstrate that the shielding performance of PMMA/Bi_2O_3/ZnO nanocomposites is strongly dependent on the interplay between photon energy, elemental composition, and the dominant radiation interaction mechanism.

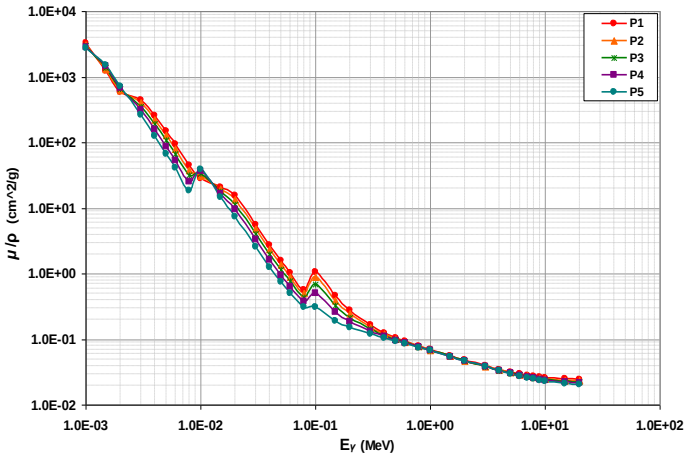


Figure 2. γ-ray energy dependent mass attenuation coefficients of the nanocomposites.

Figure 3 shows the γ-ray energy-dependent radiation protection efficiency (RPE%) of the nanocomposites. The values of RPE% were found to be sensitive to the samples' thicknesses (1, 5 and 10 cm). Generally, the RPE% values were very close to 100% for the γ-ray energies E < 0.02, 0.04 and 0.05 MeV for all the nanocomposites at various thicknesses. Furthermore, the values of this parameter became very low. The numbers of RPE% increased with increasing sample thickness for all energy values [29]. The obtained peaks at 0.09053 MeV can be ascribed to the K-absorption edge of the bismuth element.

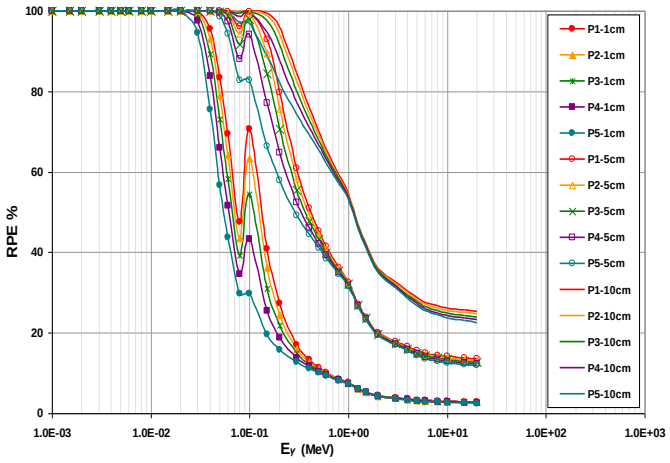


Figure 3. γ-ray energy dependent radiation protection efficiency of the nanocomposites.

Mass energy absorption coefficient

Figure 4 presents the γ-ray energy dependent mass energy absorption coefficients of the nanocomposites. It is clear that the energy dependence of μ_{en}/ρ is similar to the behavior of the μ/ρ (Figure 2), where the values of this coefficient were very large at the low energies range due to the dominance of the photoelectric effect interaction and its values are very close for all samples at the low energy range of E < 0.002 MeV. Thereafter, the values of this coefficient started rising from specimen P1 with the increase of Bi_2O_3 concentrations [43] and this is attributed to the high atomic number of bismuth (Z=83), the effect of which increases with increasing bismuth concentration in hybrid composite samples. In addition, the values of μ_{en}/ρ were decreased as became very small at energies E > 1 MeV. Irrespective of the compositions, the values of μ_{en}/ρ in the entire energy range were very close.

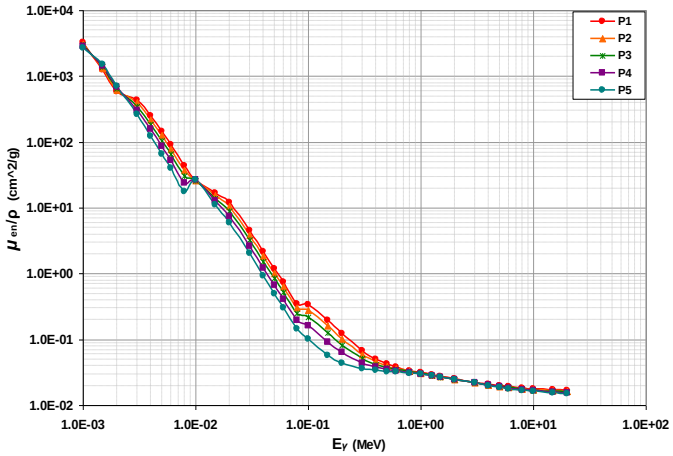


Figure 4. γ-ray energy-dependent mass energy absorption coefficients of the nanocomposites.

Specific gamma ray constant and irradiation dose rate

Figure 5 shows the gamma-ray energy-dependent specific gamma constant factor (Γ) of the nanocomposites. The reduction or weakening of the irradiation dose rate (D) in the proposed shield was evaluated by calculating Γ values using equation (7) in terms of E_γ and μ_{en}/ρ. It was assumed that the γ-ray source with activity 1 Ci was kept at a distance of 1 m from the target sample at an exposure rate of 1R/hr. The values of Γ were highest at the lowest energy of γ-rays due to the predominance of photoelectric absorption processes and the penetrating force of high-energy gamma-ray photons through the proposed nanocomposites [25, 43]. Then, the values of Γ were decreased dramatically with the increase in the γ-ray energy to approach zero at approximately 0.1 MeV. Later, the value began to increase gradually and relatively slightly for energies E > 1 MeV. It was asserted that the Bi_2O_3 incorporation into the nanocomposite shield had a significant effect on the Γ values, indicating an increase in Γ with the increase of Bi_2O_3 contents at the expense of ZnO.

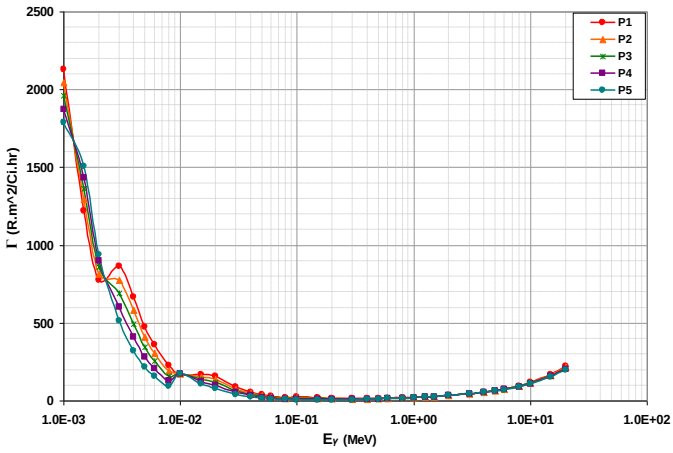


Figure 5. γ-ray energy dependent specific gamma constant factor of the nanocomposites.

Figure 6 displays the γ-ray energy-dependent irradiation dose rate of the nanocomposites. The results clearly showed that the sample type and thickness have a significant effect on the value of D absorbed by the shield. The values of D were decreased with the increase of γ-ray energy around E < 0.2 MeV. This decrease was mainly due to the reduction of Bi_2O_3 content-related highest specific value and increase in the thickness of the sample. The nanocomposite P1 as a shield achieved the best results in consuming the largest possible values for the irradiation dose rate at all energies, especially at the mid-energy region. Additionally, the values of D were close together for all samples with a specific thickness and then increased gradually with the increase of E_γ above 0.6 MeV. This increase can be attributed to the increase in the Compton scattering interactions and pair production [43].

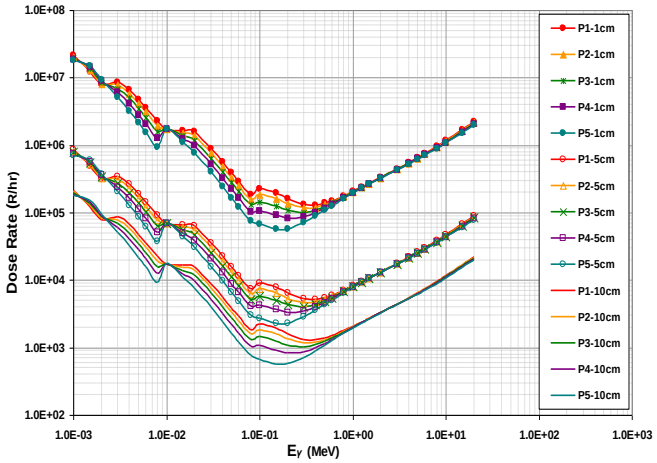


Figure 6. γ-ray energy dependent irradiation dose rate of the nanocomposites.

Electron stopping power

Figure 7 depicts the energy dependence of electron collision, radiative, and total mass stopping power for the nanocomposites. These values are the indicator of the capacity of any nuclear shield material to protect against different types of nuclear radiation. The ability of these shields to stop beta particles represented by electrons was studied using ESTRA code [44]. The values of electronic collision $((-dE/\rho dx)_{col})$, radiative $((-dE/\rho dx)_{rad})$ and total mass stopping power $(-dE/\rho dx)$ of electrons in the energy range of 0.1-100 MeV were calculated. The results displayed that the values of $(-dE/\rho dx)_{col}$ were higher at lower energies and then began to drop with the increase of electron energy. Later, the values began to gradually increase at energy above 1 MeV. In addition, the values of $(-dE/\rho dx)_{rad}$ were very small at energies less than 1 MeV. Next, the values started to increase slightly in the energy range of 1 MeV < E < 10 MeV. Later, the values were increased significantly to be greater than $(-dE/\rho dx)_{col}$ values at 5 MeV for P1 and at 6.5 MeV for P5. Also, the behavior of $-dE/\rho dx$ showed that the total mass stopping power of the electron was weak in the medium-energy region of the interacting electrons and was the greatest possible at high energies. The values were increased significantly at the energy range of E > 10 MeV which was due to the increase of bremsstrahlung probability [25]. The obtained findings were consistent with the previous reports [17-20]. In addition, the values of $-dE/\rho dx$ and $(-dE/\rho dx)_{col}$ were found to increase, and the values of $(-dE/\rho dx)_{rad}$ were decreased linearly with the increase in the Bi_2O_3 contents in the nanocomposites. The shield P1 achieved the highest value of $-dE/\rho dx$ at the high energy range, indicating an improvement in the total mass stopping power of electrons with the increase of Bi_2O_3 contents (decrease of ZnO concentration) in the nanocomposites.

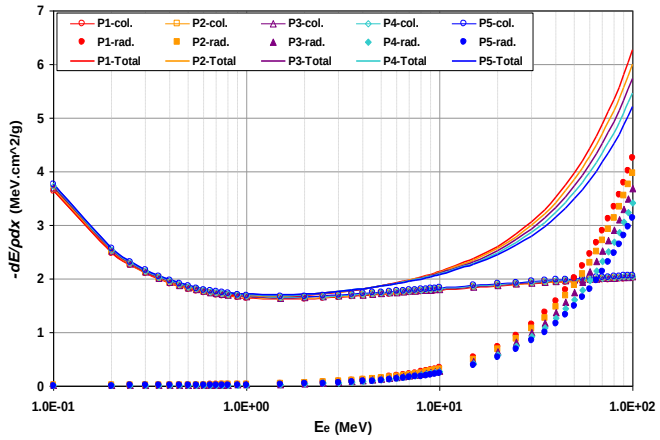


Figure 7. Energy dependence of electron collision, radiative, and total mass stopping power for the nanocomposites.

Fast neutron removal cross-section

Table 2 enlists the values of ΣR (cm^{-1}) for the fast neutrons and the weight fraction ratios in each nanocomposite calculated using equation (13). The achieved values were compared with the results of the Phy-x/PSD program calculations, indicating a perfect match between those values.It should be noted that the ΣR provided a preliminary estimation of the neutron attenuation capability of the investigated materials; however, it does not represent a complete evaluation of neutron shielding performance. A comprehensive assessment requires additional parameters, such as neutron transmission, attenuation length, and energy-dependent neutron interaction characteristics, as well as experimental validation. Therefore, the present theoretical analysis should be considered a preliminary investigation that provides valuable guidance for the design and optimization of PMMA–Bi_2O_3–ZnO nanocomposites. Further experimental studies and advanced neutron transport simulations are necessary to fully evaluate their practical potential for neutron shielding applications.

Table 2. Neutron removal cross-section of the nanocomposites.

Sample	Element	Frac. by Wt.	Frac. dens. (g/cm^3)	ΣR/ρ (cm^2/g)	ΣR (cm^{-1})	ΣR (cm^{-1}) Present Work	ΣR (cm^{-1}) Phy-x/PSD
P1	C	0.4799	0.5502	0.0502	0.0276	0.086952	0.086952
	H	0.0644	0.0739	0.5980	0.0442		
	O	0.2782	0.3189	0.0405	0.0129		
	Zn	0.0161	0.0184	0.0183	0.0003		
	Bi	0.1615	0.1851	0.0103	0.0019		
P2	C	0.4799	0.5481	0.0502	0.0275	0.087049	0.087049
	H	0.0644	0.0736	0.5980	0.0440		
	O	0.2819	0.3220	0.0405	0.0130		
	Zn	0.0482	0.0551	0.0183	0.0010		
	Bi	0.1256	0.1434	0.0103	0.0015		
P3	C	0.4799	0.5460	0.0502	0.0274	0.087146	0.087146
	H	0.0644	0.0733	0.5980	0.0438		
	O	0.2857	0.3250	0.0405	0.0132		
	Zn	0.0804	0.0914	0.0183	0.0017		
	Bi	0.0897	0.1021	0.0103	0.0011		
P4	C	0.4799	0.5440	0.0502	0.0273	0.087241	0.087241
	H	0.0644	0.0730	0.5980	0.0437		
	O	0.2894	0.3281	0.0405	0.0133		
	Zn	0.1125	0.1275	0.0183	0.0023		
	Bi	0.0538	0.0610	0.0103	0.0006		
P5	C	0.4799	0.5420	0.0502	0.0272	0.087336	0.087336
	H	0.0644	0.0728	0.5980	0.0435		
	O	0.2931	0.3311	0.0405	0.0134		
	Zn	0.1446	0.1634	0.0183	0.0030		
	Bi	0.0179	0.0203	0.0103	0.0002		

Figure 8 reveals the neutron removal cross-section of the nanocomposites. The values of ΣR for the fast neutron were found to be sensitive to the sample type. The value of ΣR was lowest (0.086952 cm^{-1}) for the nanocomposite P1; thereafter, the value of ΣR was increased until it reached the highest possible value (0.087336 cm^{-1}) for the nanocomposite P5, indicating a considerable effect of ZnO substitution in the place of Bi_2O_3 into the nanocomposites. Consequently, this caused an increase in the ability of the nanocomposites to remove fast neutrons because the materials with small atomic numbers have a larger cross-section for the interaction of neutrons [37, 44]. Thus, the proposed nanocomposites were shown to be more efficient in reducing the fast neutrons than boron carbide (ΣR = 0.071 cm^{-1}) [45], graphite (ΣR = 0.077 cm^{-1}) [25, 45], and polyethylene grains (ΣR = 0.078 cm^{-1}) [45].

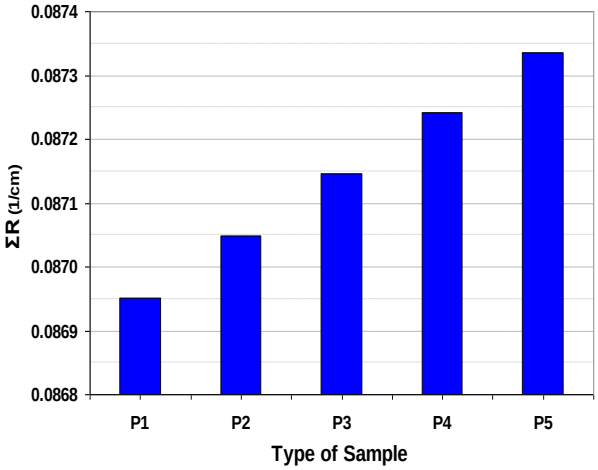


Figure 8. Neutron removal cross-section of the nanocomposites.

Conclusions

This paper reported the gamma-ray, electron, and fast neutrons shielding parameters of five theoretically formulated PMMA/Bi_2O_3/ZnO nanocomposites. The calculations showed that increasing the Bi_2O_3 content increased the calculated gamma-ray attenuation parameters and total electron mass stopping power, particularly in energy regions where high-Z constituents contribute strongly to photon interactions and radiative electron energy loss. The NIST Standard Reference Database 126, ESTRA code, and Phy-x/PSD online program were used for the detailed assessment of shielding characteristics of the studied nanocomposites and further comparison with other materials. The values of radiation shielding efficiency, specific γ-ray constant, irradiation dose rate, and fast neutron removal cross-section were obtained, analyzed and compared. Compared to other conventional commercial materials (boron carbide, graphite, and polyethylene grains), the reported nanocomposites demonstrated better radiation shielding abilities. Especially, nanocomposites P1 and P5 disclosed the optimum shielding potential against γ-rays and fast neutrons, respectively. It was asserted that the ionizing radiation shielding capacity of the studied nanocomposites can be specific by carefully adjusting the concentration of Bi_2O_3 and ZnO nanopowders. The achieved results were interpreted in terms of molecular weights of Bi_2O_3 and ZnO, Compton effect, pair production, and photoelectric effect. Based on the results, it was established that the proposed novel nanocomposites may be advantageous for high-performance shielding material manufacturing required for a broad array of uses in different sectors and environmental remediation.

Acknowledgment

This research was funded by RMC UTM, grant Vot. No. 23H48 and Malaysia Ministry of Higher Education under the Prototype Research Grant Scheme Phase 1/2025 with the reference number PRGS/1/2025/TK09/UTM/02/1.

Conflicts of Interest

The following authors are affliated with organizations that have a direct or indirect financial interest in the subject matter covered in the manuscript.

Ethical Approval

All authors made substantial contributions to the conception and design of the study, the analysis and interpretation of data, the drafting of the manuscript or its critical revision for important intellectual

content, and the final approval of the version to be published.

References

[1] S. Gupta, G. S. Sidhu, *Int. J. Sci. Res.* 2 (2012) 1.
[2] M. J. Aldhuhaibat, M. S. Amana, N. J. Jubier, A. A. Salim, *Radiat. Phys. Chem.* 179 (2021) 109183.
[3] M. S. Amana, M. J. R. Aldhuhaibat, A. A. Salim, *SCIOL Biomed.* 4 (2021) 191.
[4] M. S. Al-Buriahi, C. Eke, S. Alomairy, A. Yildirim, H. I. Alsaeedy, C. Sriwunkum, *Polym. Adv. Technol.* 32 (2021) 2386.
[5] M. S. Al-Buriahi, M. Hessien, F. Alresheedi, A. M. Al-Baradi, Z. A. Alrowaili, I. Kebaili, I. O. Olarinoye, *Ceram. Int.* 48 (2022) 3464.
[6] J. S. Alzahrani, Z. A. Alrowaili, H. H. Saleh, A. Hammoud, S. Alomairy, C. Sriwunkum, M. S. Al-Buriahi, *Prog. Nucl. Energy* 142 (2021) 103992.
[7] A. E. S. Abdo, M. A. M. Ali, M. R. Ismail, *Radiat. Phys. Chem.* 66 (2003) 185.
[8] M. J. Aldhuhaibat, M. S. Amana, H. Aboud, A. A. Salim, *Ceram. Int.* 48 (2022) 25011.
[9] M. Sheela, V. A. Kamat, K. U. Kiran, K. M. Eshwarappa, *Radiat. Prot. Environ.* 42 (2019) 180.
[10] N. M. Aowd, H. S. Hussain, *Eng. Technol. J.* 33 (2015) 1.
[11] Z. Li, S. Chen, S. Nambiar, Y. Sun, M. Zhang, W. Zheng, J. T. Yeow, *Nanotechnology* 27 (2016) 234001.
[12] T. Bel, C. Arslan, N. Baydogan, *Mater. Chem. Phys.* 221 (2019) 58.
[13] D. Cao, G. Yang, M. Bourham, D. Moneghan, *Nucl. Eng. Technol.* 52 (2020) 2613.
[14] H. Gümüş, F. Köksal, *Radiat. Eff. Defects Solids* 157 (2002) 445.
[15] S. Tanuma, C. J. Powell, D. R. Penn, *Surf. Interface Anal.* 37 (2005) 978.
[16] Z. Tan, Y. Xia, *Appl. Radiat. Isot.* 70 (2012) 296.
[17] M. O. El-Ghossain, *Int. J. Phys.* 5 (2017) 92.
[18] M. O. El-Ghossain, *Int. J. Sci. Technol. Res.* 6 (2017) 114.
[19] M. J. Aldhuhaibat, H. S. Farhan, R. H. Hassani, H. M. Tuma, H. Bakhtiar, A. A. Salim, *Appl. Phys. A* 128 (2022) 1058.
[20] H. K. Yasser, M. J. Aldhuhaibat, A. J. Farhan, in: *AIP Conference Proceedings*, AIP Publishing, Melville, NY, 2024, p. 190001.
[21] N. J. AbuAlRoos, M. N. Azman, N. A. B. Amin, R. Zainon, *Phys. Med.* 78 (2020) 48.
[22] L. Gerward, N. Guilbert, K. B. Jensen, H. Levring, *Radiat. Phys. Chem.* 60 (2001) 23.
[23] L. M. Unger, D. K. Trubey, Specific Gamma-Ray Dose Constants for Nuclides Important to Dosimetry and Radiological Assessment, Oak Ridge National Lab., Oak Ridge, TN, 1982, p. 1.
[24] S. F. Hathot, N. J. Jubier, R. H. Hassani, A. A. Salim, *Optik* 247 (2021) 167941.
[25] H. Aboud, M. J. Aldhuaibata, Y. Alajermi, *J. Phys. Chem. Solids* 164 (2022) 110597.
[26] G. Dutta, D. Bose, *Int. J. Emerg. Technol. Adv. Eng.* 2 (2012) 121.
[27] E. Şakar, Ö. F. Özpolat, B. Alım, M. I. Sayyed, M. Kurudirek, *Radiat. Phys. Chem.* 166 (2020) 108496.
[28] N. Y. M. Isa, E. S. Sazali, R. Hisam, S. K. Ghoshal, S. K. M. Zain, N. H. Juma'ln, A. Awang, in: *Journal of Physics: Conference Series*, IOP Publishing, Bristol, UK, 2021, p. 012027.
[29] H. C. Manjunatha, L. Seenappa, B. M. Chandrika, C. Hanumantharayappa, *Ann. Nucl. Energy* 109 (2017) 310.
[30] M. J. Berger, ESTAR, PSTAR, ASTAR: A PC Package for Calculating Stopping Powers and Ranges of Electrons, Protons and Helium Ions, International Atomic Energy Agency, Vienna, 1993, p. 1.
[31] National Research Council, Health Effects of Exposure to Low Levels of Ionizing Radiation: BEIR V, National Academies Press, Washington, DC, 1990, p. 1.
[32] S. N. Ahmed, Physics and Engineering of Radiation Detection, Academic Press, San Diego, CA, 2007, p. 1.
[33] A. A. Salim, S. K. Ghoshal, H. Bakhtiar, *Optik* 226 (2021) 165879.
[34] Y. H. Song, Y. N. Wang, *Nucl. Instrum. Methods Phys. Res. Sect. B* 135 (1998) 124.
[35] F. A. Mettler, Medical Effects of Ionizing Radiation, W.B. Saunders, Philadelphia, PA, 1985, p. 1.
[36] Y. Elmahroug, B. Tellili, C. Souga, *Int. J. Phys. Res.* 3 (2013) 7.
[37] J. Wood, Computational Methods in Reactor Shielding, Elsevier, Oxford, 2013, p. 1.
[38] M. U. Khan, S. Ahmad, A. A. Naqvi, H. J. Al-Gahtani, *Prog. Nucl. Energy* 130 (2020) 103550.
[39] M. S. Amana, N. J. Jubier, M. J. Aldhuhaibat, A. A. Salim, *Radiat. Detect. Technol. Methods* 5 (2021) 633.
[40] Ö. F. Özpolat, B. Alım, E. Şakar, M. Büyükyıldız, M. Kurudirek, *Radiat. Environ. Biophys.* 59 (2020) 321.
[41] J. H. Hubbell, S. M. Seltzer, Tables of X-Ray Mass Attenuation Coefficients and Mass Energy-Absorption Coefficients 1 keV to 20 MeV for Elements Z=1 to 92 and 48 Additional Substances of Dosimetric Interest, National Institute of Standards and Technology, Gaithersburg, MD, 1995, p. 1.
[42] H. C. Manjunatha, L. Seenappa, B. M. Chandrika, K. N. Sridhar, C. Hanumantharayappa, *Appl. Radiat. Isot.* 139 (2018) 187.
[43] M. J. Berger, J. S. Coursey, M. A. Zucker, J. Chang, Stopping-Power and Range Tables for Electrons, Protons, and Helium Ions, National Institute of Standards and Technology, Gaithersburg, MD, 2017, p. 1.
[44] F. Fernandez-Alonso, D. L. Price, Neutron Scattering, Academic Press, Boston, MA, 2013, p. 1.
[45] P. Kaur, K. J. Singh, S. Thakur, in: *Journal of Physics: Conference Series*, IOP Publishing, Bristol, UK, 2020, p. 012043.